Electronic Supporting Information

The synthesis and structural aspects of the perbromo-functionalised thiaboranes *closo*-SB_nBr_n (n = 5, 9, 11): the solid-state structure of the octahedral *closo*-SB_5Br_5, governed by strong dihalogen contacts

Willi Keller,[*a] Joachim Ballmann,[b] Jindřich Fanfrlík,[c] and Drahomír Hnyk[*d]

[a] Institut für Chemie, Universität Hohenheim, Garbenstrasse 30, 70599 Stuttgart, Germany

[b] Anorganisch-Chemisches Institut, Ruprecht-Karls-Universität Heidelberg, Im Neuenheimer Feld 270, 69120 Heidelberg, Germany

[c] Institute of Organic Chemistry and Biochemistry of the Czech Academy of Sciences, Flemingovo nám. 2, 166 10 Praha 6, Czech Republic

[d] Institute of Inorganic Chemistry of the Czech Academy of Sciences, CZ-250 68 Husinec-Řež, Czech Republic

Experimental Section

Instrumentation

NMR spectra were recorded either on a Bruker AVANCE III HD 600 (^{11}B 192.552 MHz). All ^{11}B chemical shifts are referenced to external $BF_3{\cdot}OEt_2$. The NMR spectra were processed using SpinWorks 4 (v 4.2.3.0 Kirk Marat, University of Manitoba, Canada) software. High- and low-resolution mass spectra were obtained on a Thermoscientific Exactive GC with electron ionization at 70 eV.

General Procedures and Materials

All manipulations were conducted using standard high vacuum or inert atmosphere techniques as described by *Shriver*.[1] Solvents were reagent grade, dried and purified according to standard procedures. BBr_3 was stirred over mercury, degassed, and condensed into a trap of −78 °C prior to use. Diboron tetrabromide B_2Br_4 was prepared by co-condensing BBr_3 and vaporized Cu onto cooled walls (−196 ºC) of a metal-vapor reactor similar to that

described by Timms.[2] After reaction, B_2Br_4 was separated from excess BBr_3 by repeated fractionation until the condensate exhibited a vapor pressure of less than 1 Torr at 0 °C. Further information including figures depicting the copper-vaporisation and working technique with the standard-vacuum line can be found in the Supporting Information of a recent article.[3]

Synthesis of S_2Br_2: S_2Br_2 is not available commercially, but can be readily prepared by adapting the standard method[4] to vacuum conditions, according to equation ¼ S_8 + Br_2 → S_2Br_2.

0.3 g (1.17 mmol) elemental S_8 0.75 g (1.17 mmol) and 0.75 g (4.69 mmol) of elemental Br_2 were filled into an a 100 mL Pyrex-glass flask equipped with a right-angle PTFE high-vacuum valve (J. Young Scientific Glassware, Acton, London) and an O-ring seal for greaseless connection to the vacuum-line. After evacuating (10^{-3} mbar), the reaction mixture was heated over-night (ca. 20 h) at T = 120 °C resulting in a complete consumption of the elemental sulphur and the formation of a red-brown liquid. Traces of unreacted Br_2 were pumped-off from the flask at −40 °C and fractionation at room temperature gave in almost quantitative yield 1.0 g of pure S_2Br_2 as a red-brown liquid (lit.[4] bp. 46−48 °C/10^{-1} Torr, mp. −46 °C).

Synthesis of *closo*-SB_5Br_5 (1), ***closo*-1-SB_9Br_9 (2)**, and ***closo*-$SB_{11}Br_{11}$ (3):** In a typical pyrolysis, 0.4 g S_2Br_2 (1.78 mmol) was condensed *in vacuo* (10^{-3} mbar) into a 2 x 500-mL double-flask system equipped with a seal-constriction and a break-seal joint (see Figure S18). Thereafter, 6.51 g B_2Br_4 (19.08 mmol) was condensed separately into the other of both flasks. The sealed double-flask was brought into an preheated oven of 350 °C and allowed to slowly cool to room temperature over a period of 20 h resulting in rusty-brown solid together with colorless (thiaboranes) and red B_9Br_9 crystals. After opening of the break-seal under vacuum, ca. 15 ml BBr_3 was condensed into one of the flasks in order to thoroughly extract the solid

products from the flasks repeatedly 10 times into a separate flask. The part which was insoluble in BBr_3 was separated by a frit and the residue repeatedly was extracted 5 times with 15 ml BBr_3 until the color of the extract disappeared. After evaporation of the extractant BBr_3 at temperatures below 20 °C, the residue was separated under dynamic vacuum (10^{-3} mbar) by fractional sublimation. SB_5Br_5 (**1**) sublimed as off-white solid at $T_{subl.}$ 40 ºC (ca. 35 mg). Further purification was achieved by repeated vacuum-sublimation/crystallisation processes.

Data for *closo*-SB_5Br_5 (**1**): EI-MS *m/z* (rel. int.): 486 (100, M^+); 406 (1, $[M\text{-}Br]^+$); 363 (35, $[M\text{-}SBBr = B_4Br_4]^+$); 282 (13, $[B_4Br_3]^+$); 235 (32, $[M\text{-}BBr_3]^+$); 193 (15, $[B_3Br_2]^+$); 171 (10, $[BBr_2]^+$); exact mass calcd for $^{32}S^{11}B_5{}^{79}Br_5$ 485.6076; found 485.6075; fragments: calcd for $^{11}B_4{}^{79}Br_4$ 363.7069; found 363.7057; calcd for $^{11}B_4{}^{79}Br_3$ 281.7933; found 282.7931; calcd for $^{32}S^{11}B_4{}^{79}Br_3$ 234.8471; found 234.8469; ^{11}B NMR (ppm, C_6D_6) 19.4 (B6), −2.3 quartet (B2-5) with cross-peak in $^{11}B^{11}B$ COSY NMR.

Data for *closo*-1-SB_9Br_9 (**2**): MS *m/z* (rel. int.): 848 (100, M^+); 816 (11, $[M\text{-}S]^+$); 768 (15, $[M\text{-}Br]^+$); 598 (28, $[M\text{-}BBr_3]^+$); exact mass calcd for $^{32}S^{11}B_9{}^{79}Br_9$ 848.3178; found 848.3182; ^{11}B NMR (ppm, C_6D_6) 49.6 (B(10)), 7.5 (B(2-5)), −3.7 (B(6-9)) with crosspeaks in $^{11}B^{11}B$ COSY NMR between B(6-9), B(10) and B(2-5).

Data for *closo*-$SB_{11}Br_{11}$ (**3**): MS *m/z* (rel. int.): 1030 (100, M^+); 950 (33, $[M\text{-}Br]^+$); 859 (3, $[M\text{-}BBr_2]^+$); 779 (6, $[M\text{-}BBr_3]^+$); 656 (5, $[M\text{-}SB_2Br_4]^+$); 576 (5, $[M\text{-}SB_2Br_5]^+$); exact mass calcd for $^{32}S^{11}B_{11}{}^{79}Br_{11}$ 1030.1719; found 1030.1717; ^{11}B NMR (ppm, C_6D_6) 14.2 (B(12)), −1.4 (B(2-6)), −3.7 (B(7-11)) with crosspeaks in $^{11}B^{11}B$ COSY NMR between B(7-11), B(12) and B(2-6).

Computational Details

1, **2**, and **3** were optimized at the B3LYP/6-311+G** level using the Gaussian09.[5] The subsequent NMR computations were performed using these geometries with the Amsterdam

Density Functional (ADF) code[6] employing the PBE0 functional. The two-component relativistic zeroth-order regular approximation (ZORA) method[7] including scalar and spin-orbit (SO)[8] corrections was employed for these computations; the all-electron triple-zeta basis set plus one polarization function (denoted TZ2P; from the ADF library) was used for all atoms. Magnetic shieldings were converted into relative ^{11}B chemical shifts using ^{11}B NMR of B_2H_6[9] as the primary references. Electrostatic potentials were computed on 0.001 a.u. at the HF/cc-pVDZ level Molekel4.3[10] programs. It has recently been shown that this basis set size is sufficient for these purposes.[11] The IAO/IBO method[12] was used to connect quantitative SCF wave functions to a qualitative chemical picture, the nature of the orbitals naturally emerges. The IBOview program was used.[12] The corresponding input files for the latter were generated at the B3LYP/def2-TZVP//B3LYP/6-311+G** level using the Turbomole6.6[13] program package.

X-Ray Crystal Structure Determination

Crystal data and details of the structure determination are compiled in Table S1. Full shells of intensity data were collected at 120(1) K with an Agilent Technologies Supernova-E CCD diffractometer (Mo-K_α radiation, microfocus X-ray tube, multilayer mirror optics). Detector frames (typically ω-, occasionally φ-scans, scan width 0.5°) were integrated by profile fitting.[14,15] Data were corrected for air and detector absorption, Lorentz and polarization effects[16] and scaled essentially by application of appropriate spherical harmonic functions.[16,17] Absorption by the crystal was treated numerically (Gaussian grid).[18] An illumination correction was performed as part of the numerical absorption correction.[16]

Using OLEX2,[19] the structure was solved with SHELXT[20] (intrinsic phasing) and refined with SHELXL[21] by full-matrix least squares methods based on F^2 against all unique reflections. All atoms were given anisotropic displacement parameters.

Note: The monoclinic angle β in crystals of B_5Br_5S is very close to 90° (see Table S1), which is commonly regarded as an indicator for higher symmetry. Indexing and integration in various orthorhombic space groups, however, lead to very large standard uncertainties for the cell axes and to unreasonably high R_{int} values of > 0.66. In $P2_1/c$, an R_{int} value of approximately 0.05 was determined. No higher symmetries were found using *ADDSYM* as implemented in PLATON.[22]

CCDC 2403282 contains the supplementary crystallographic data for this paper. These data can be obtained free of charge from the Cambridge Crystallographic Data Centre's and FIZ Karlsruhe's joint Access Service via https://www.ccdc.cam.ac.uk.

Table S1. Crystal data and details of the structure determination for B_5Br_5S.

Empirical formula	B_5Br_5S
Formula weight	485.66
Crystal system	*monoclinic*
Space group (number)	$P2_1/c$ (14)
a [Å]	18.6919(2)
b [Å]	12.52450(10)
c [Å]	13.22370(10)
β [°]	90.0170(10)
Volume [Å^3]	3095.76(5)
Z	12
ρ_{calc} [gcm^{-3}]	3.126
μ [mm^{-1}]	19.600
F(000)	2592
Radiation	Mo-K_α (λ = 0.71073 Å)

2θ range [°]	5.0 to 68.3 (0.63 Å)
Index ranges (h, k, l)	−29 to +28, ±19, ±20
Reflections collected	102152
Independent reflections	12413 (R_{int} = 0.0469)
Completeness to θ = 25.242°	99.9 %
Data / Restraints / Parameters	12413 / 0 / 299
Transmission factors (min / max)	0.704 / 1.000
Goodness-of-fit on F^2	1.024
Final R indexes [$I \geq 2\sigma(I)$]	R_1 = 0.0233, wR_2 = 0.0464
Final R indexes [all data]	R_1 = 0.0362, wR_2 = 0.0499
Largest peak/hole [eÅ^{-3}]	0.67 / −0.67
Extinction coefficient	0.000206(10)
CCDC number	2403282

In the caption of Figure 3 (see the main text), it is mentioned that three independent molecules are present in the asymmetric unit. Hence, overall 12 molecules are present in the cell. The three independent molecules and the cell axes are shown in Figure S1.

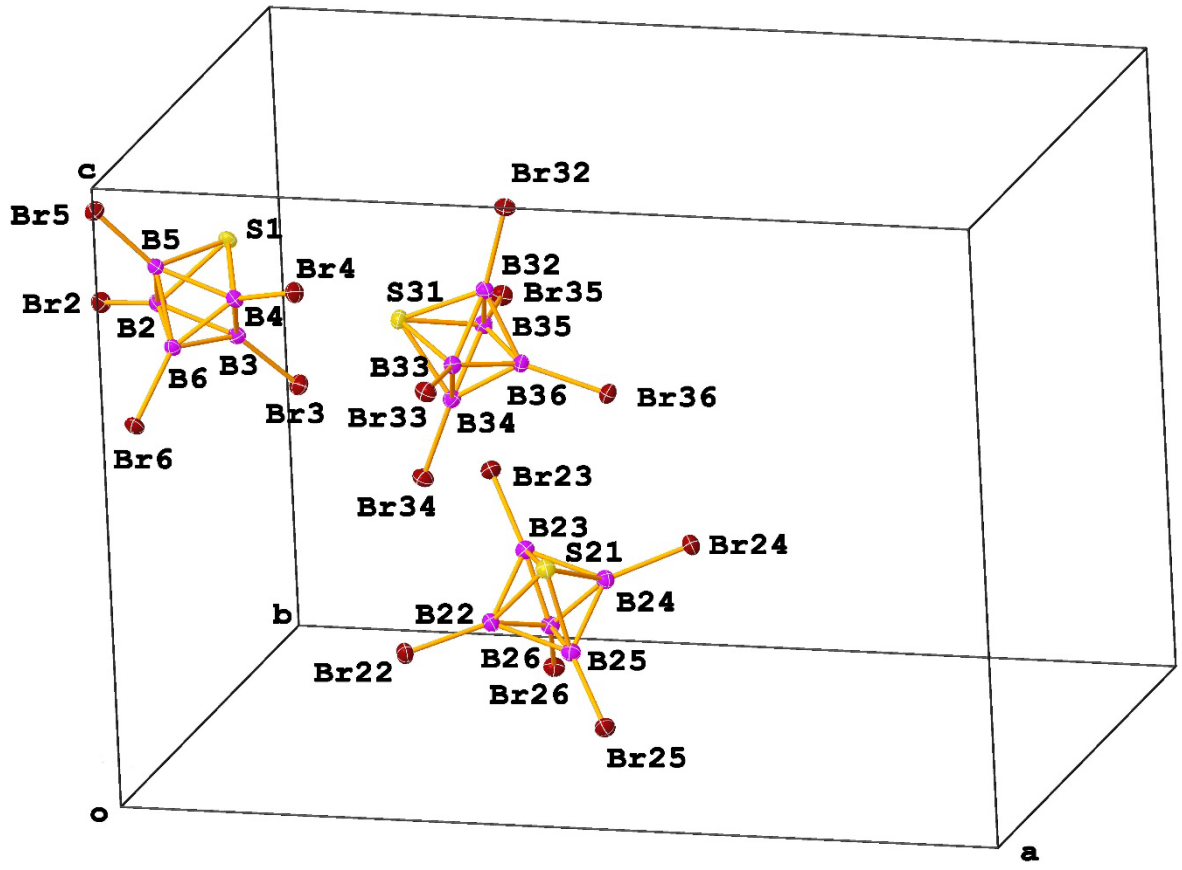

Figure S1. ORTEP plot of the three independent molecules in the asymmetric unit (thermal displacement ellipsoids drawn at the 50% probability level).

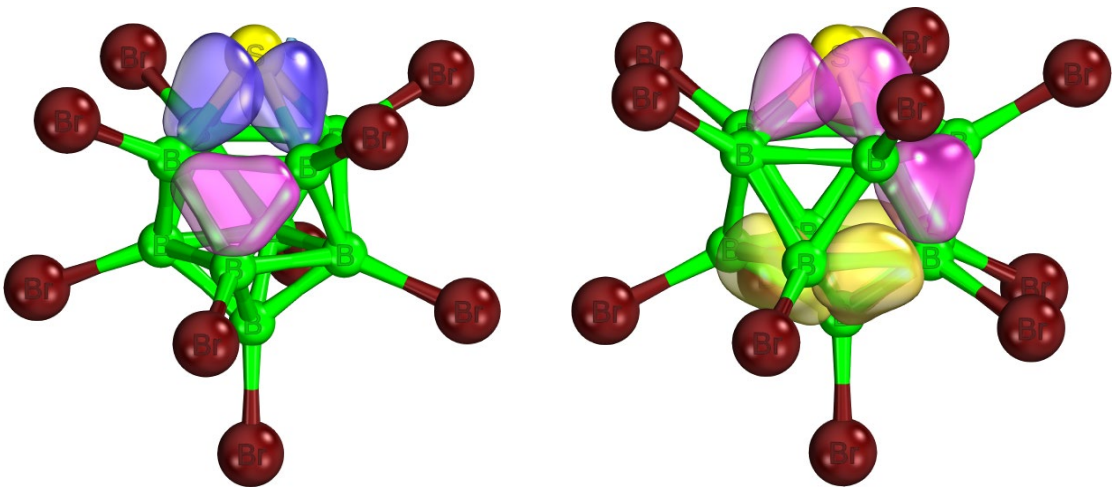

a) **b)**

Figure S2. Visualized examples of IBOs for a) *closo*-1-SB_9Br_9 (**2**) and b) *closo*-$SB_{11}Br_{11}$ (**3**). The colour coding is as follows: blue – classical 2c-2e bonding, pink – 3c-2e bonding, yellow – 4c-2e bonding.

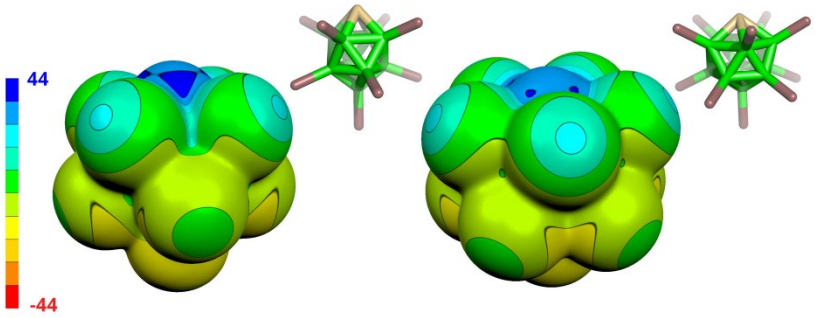

Figure S3. The computed electrostatic-potential (ESP) molecular surface of *closo*-1-SB_9Br_9 (**2**, left) and *closo*-$SB_{11}Br_{11}$ (**3**, right). The ESP colour range is in $kcal.mol^{-1}$.

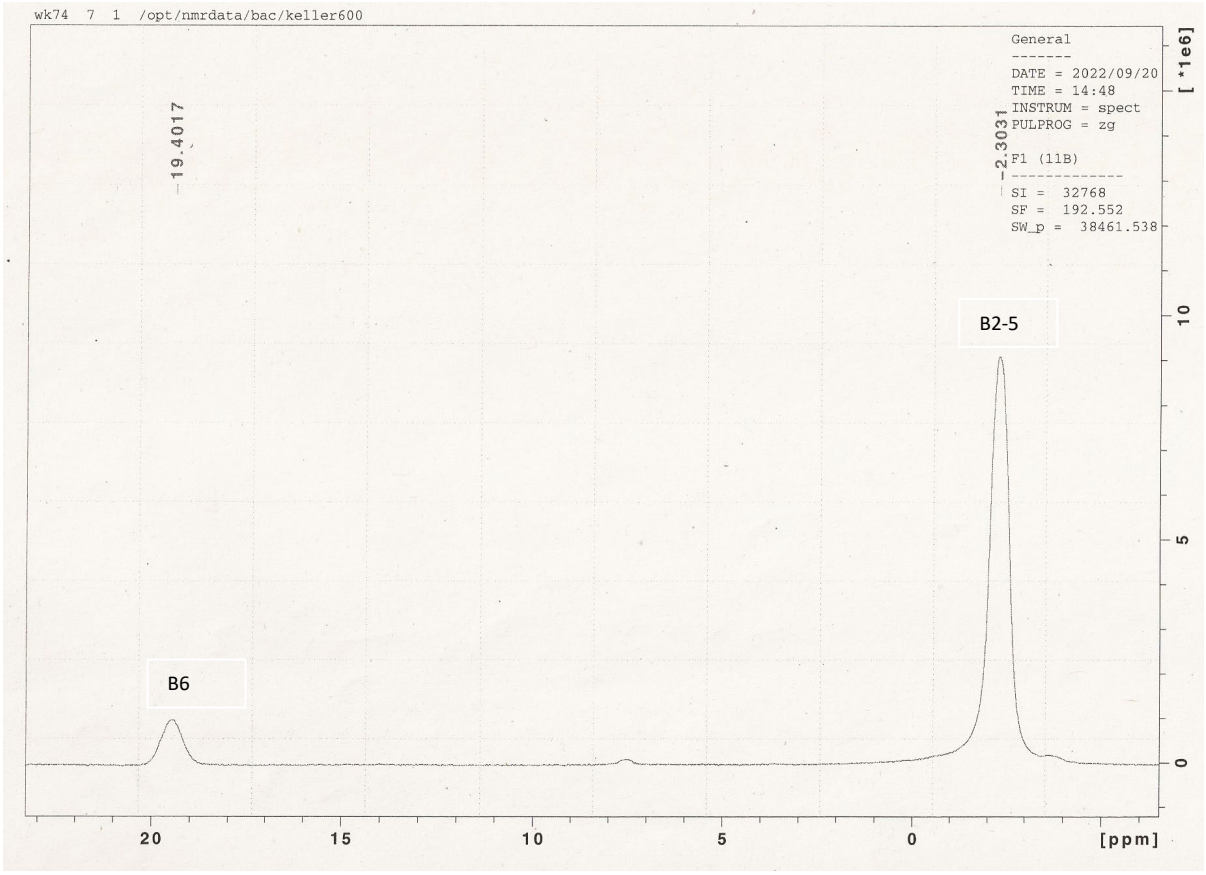

Figure S4. 192.55 MHz ^{11}B NMR spectrum of *closo*-SB_5Br_5 (**1**).

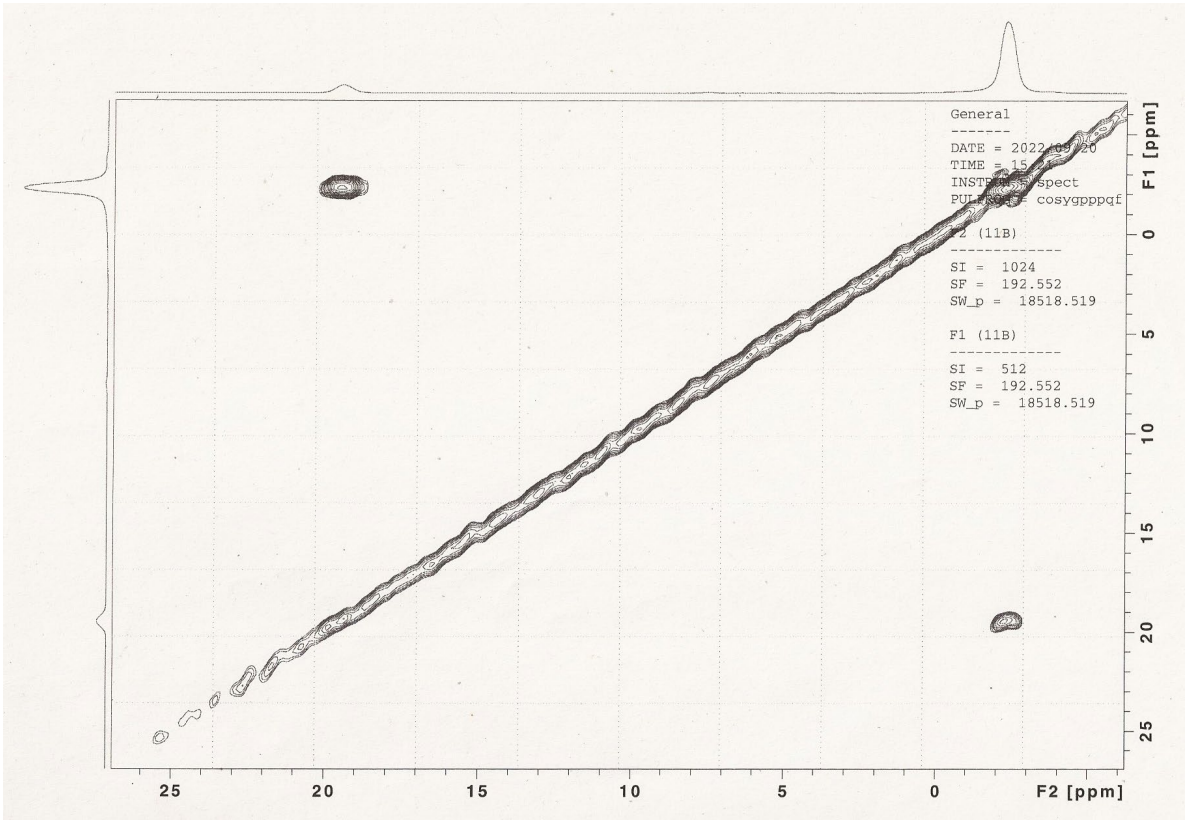

Figure S5. 192.55 MHz ^{11}B^{11}B COSY NMR spectrum of *closo*-SB_5Br_5 (**1**).

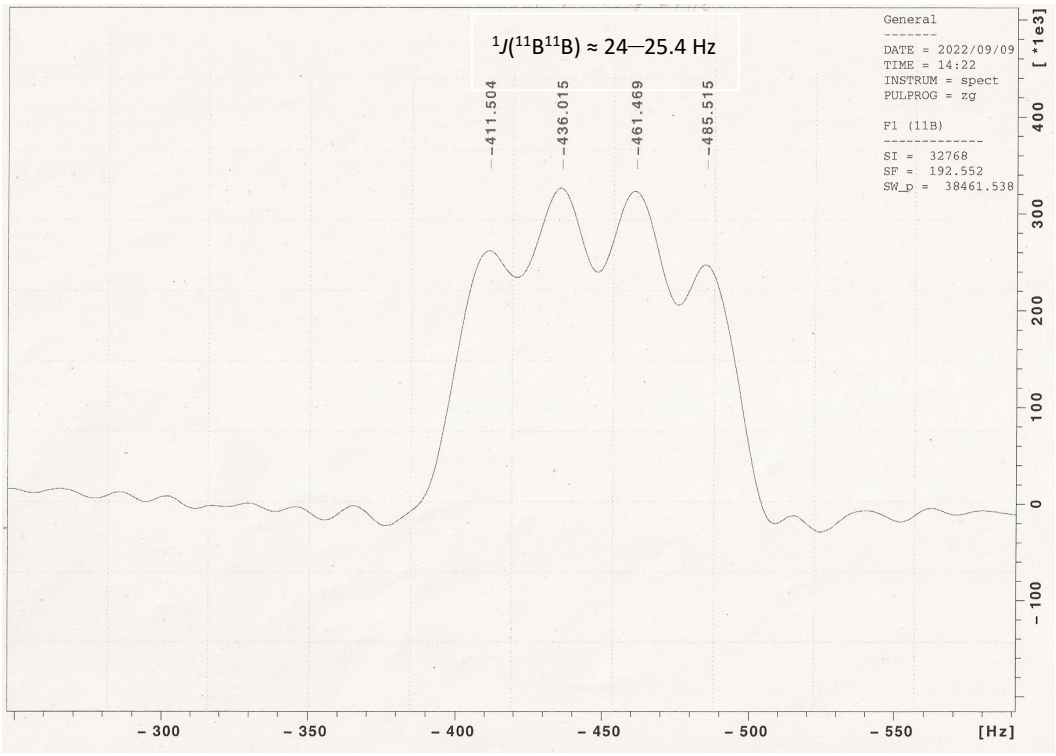

Figure S6. Resolution of $^1J(^{11}B^{11}B)$ by applying Gaussian line broadening on the signal for B(2–5) at –2.3 ppm in the 192.55 MHz ^{11}B NMR spectrum of *closo*-SB_5Br_5 (**1**) resolving the coupling to B(6).

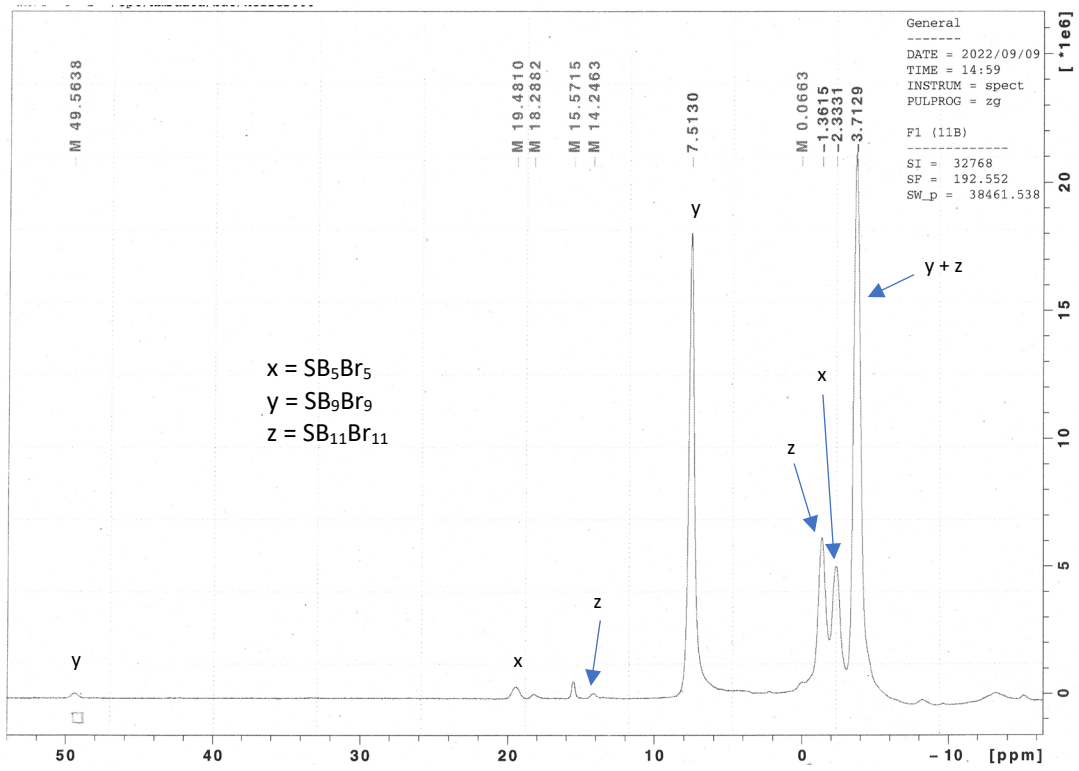

Figure S7. 192.55 MHz ^{11}B NMR spectrum of a C_6D_6 extract of the non-volatile (HV) residue of the pyrolysate (after the volatiles were pumped off 10 minutes at 300 °C) containing *closo*-SB_5Br_5 (**1**), *closo*-1-SB_9Br_9 (**2**), and *closo*-$SB_{11}Br_{11}$ (**3**). The formulas and relative amounts of the contents were analysed by EI-MS.

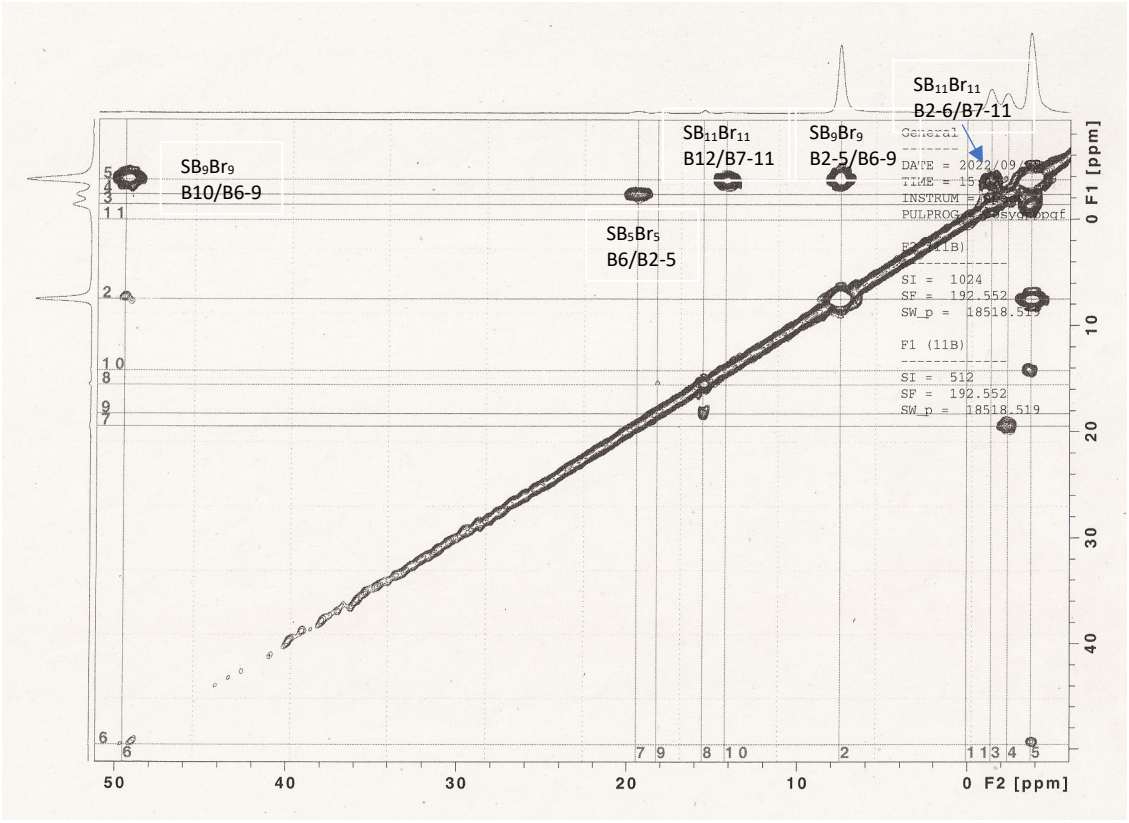

Figure S8. 192.55 MHz $^{11}B^{11}B$ COSY NMR spectrum of the sample shown in Fig. S7.

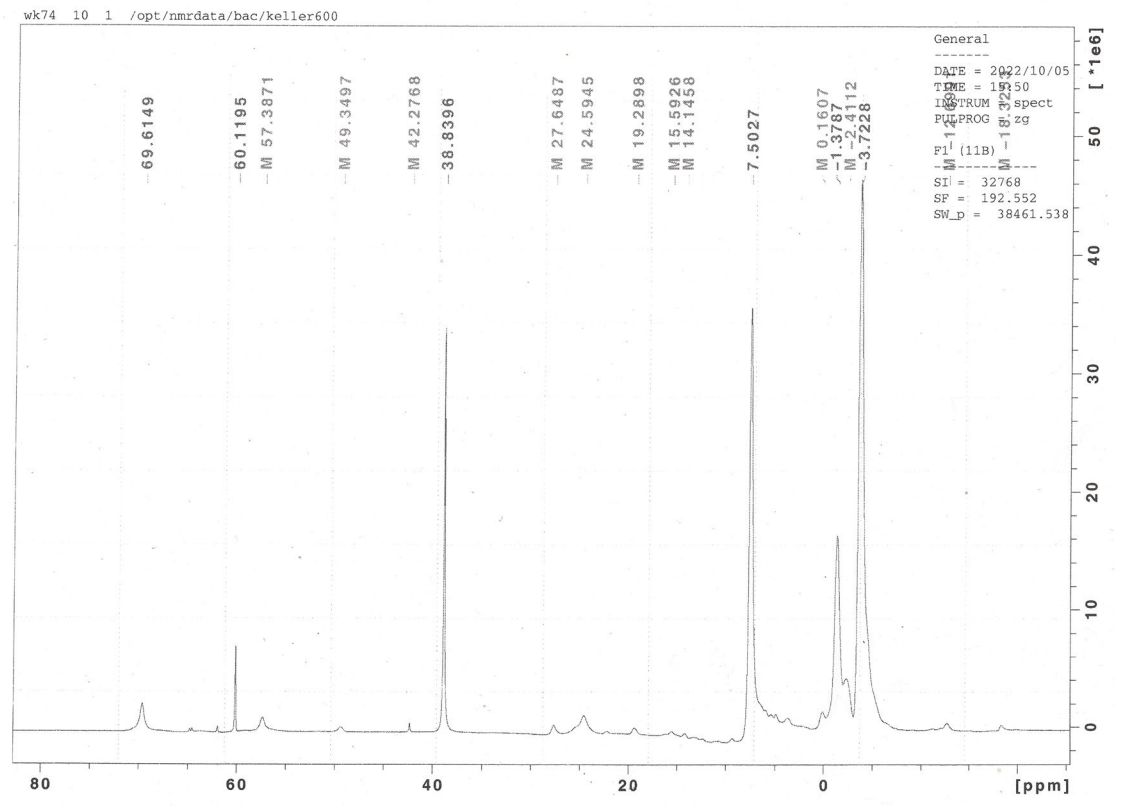

Figure S9. 192.55 MHz $^{11}B^{11}B$ COSY NMR spectrum of a C_6D_6 extract of the pyrolysate from a co-pyrolysis at 430 °C.

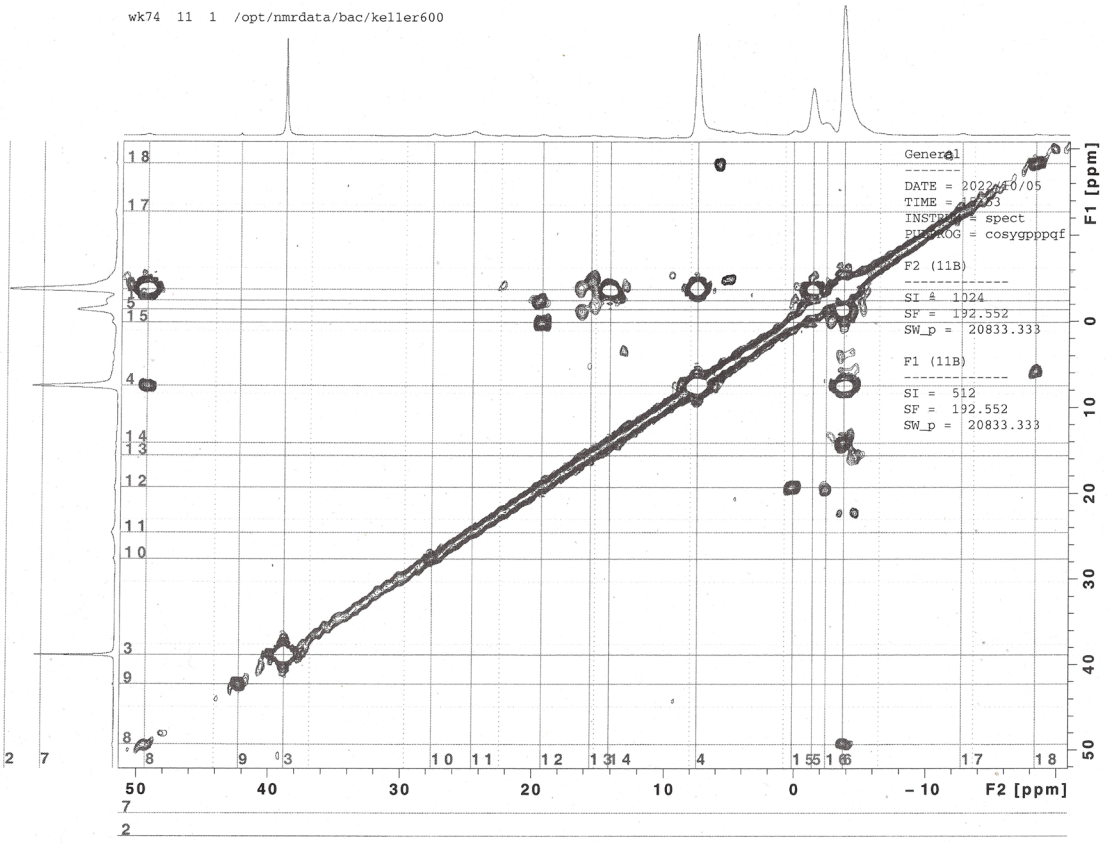

Figure S10. 192.55 MHz $^{11}B^{11}B$ COSY NMR spectrum of the sample from Fig. S9 with cross-peaks of **1**, **2**, **3** and signals of components which could not be assigned.

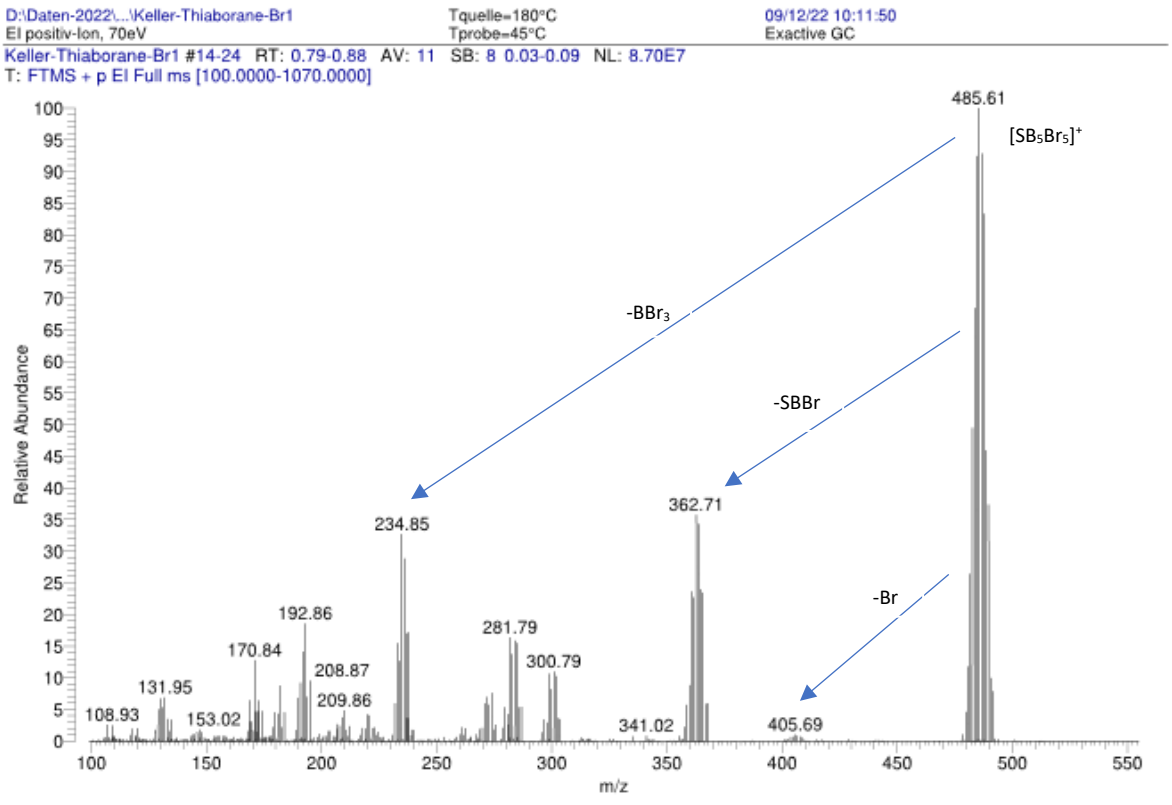

Figure S11. EI-MS (70 eV) of *closo*-SB_5Br_5 (**1**).

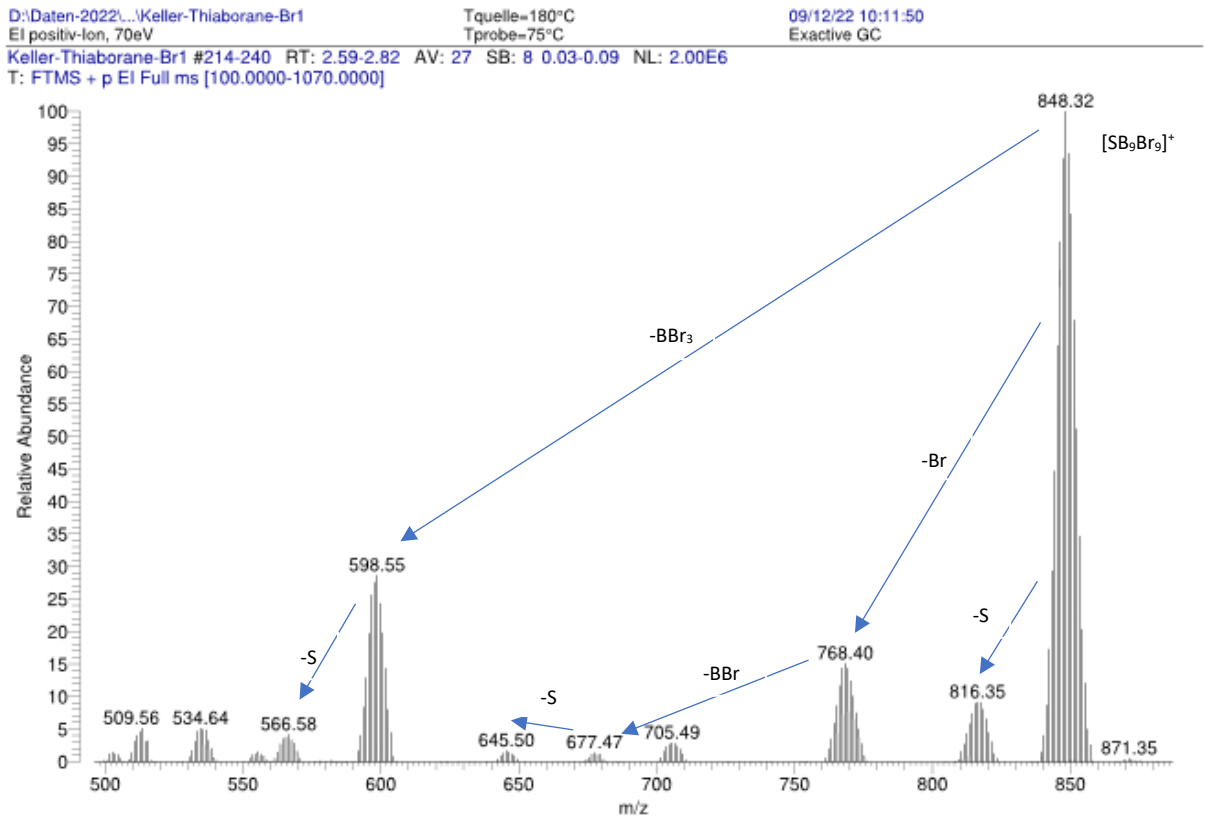

Figure S12. EI-MS (70 eV) of *closo*-1-SB_9Br_9 (**2**).

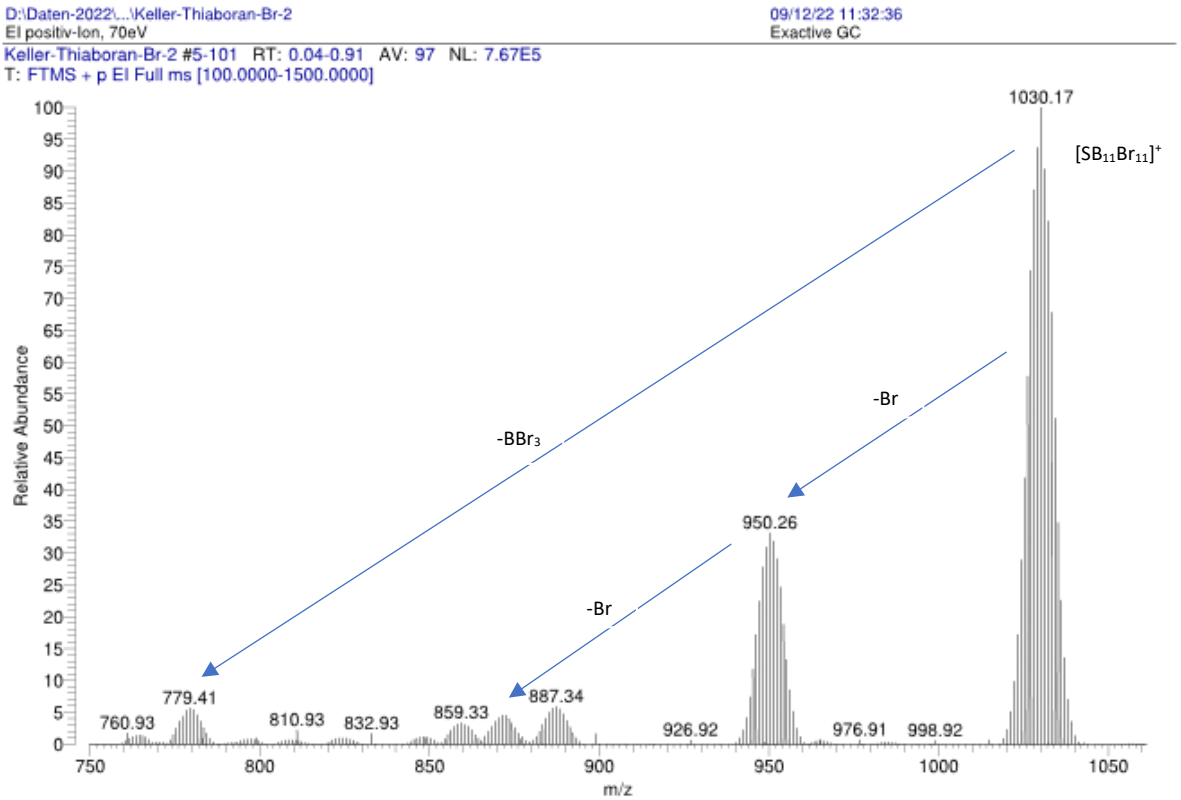

Figure S13. EI-MS (70 eV) of *closo*-$SB_{11}Br_{11}$ (**3**).

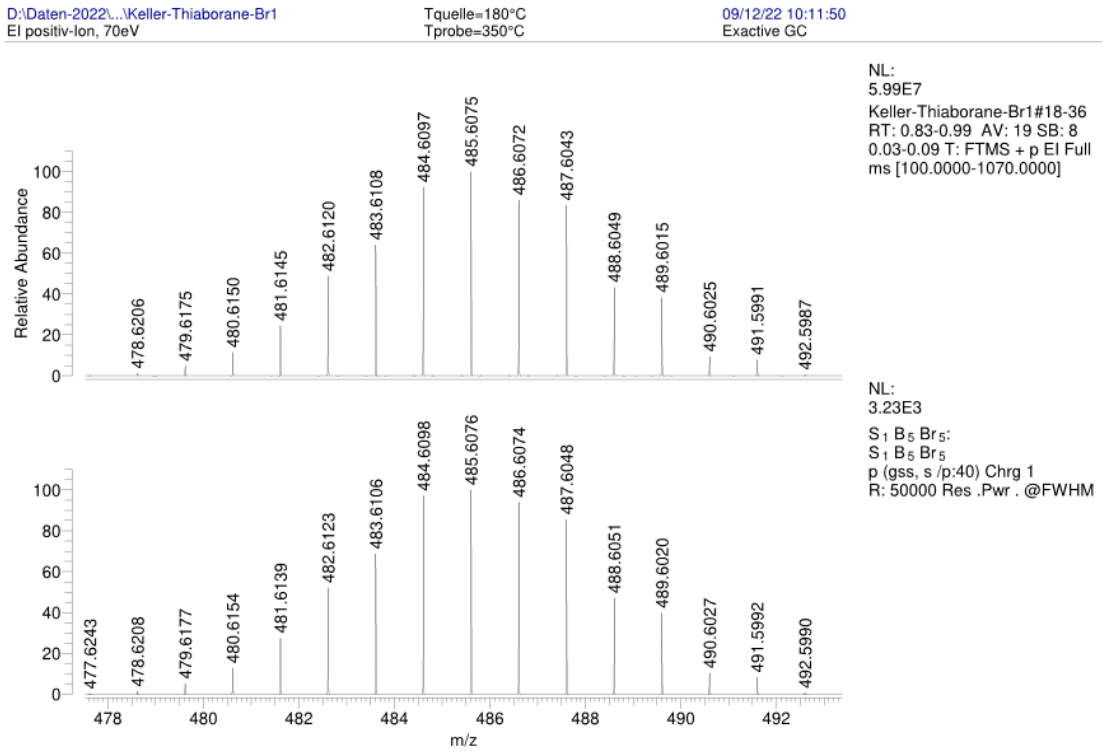

Figure S14. High resolution EI-MS of *closo*-SB_5Br_5 (**1**).

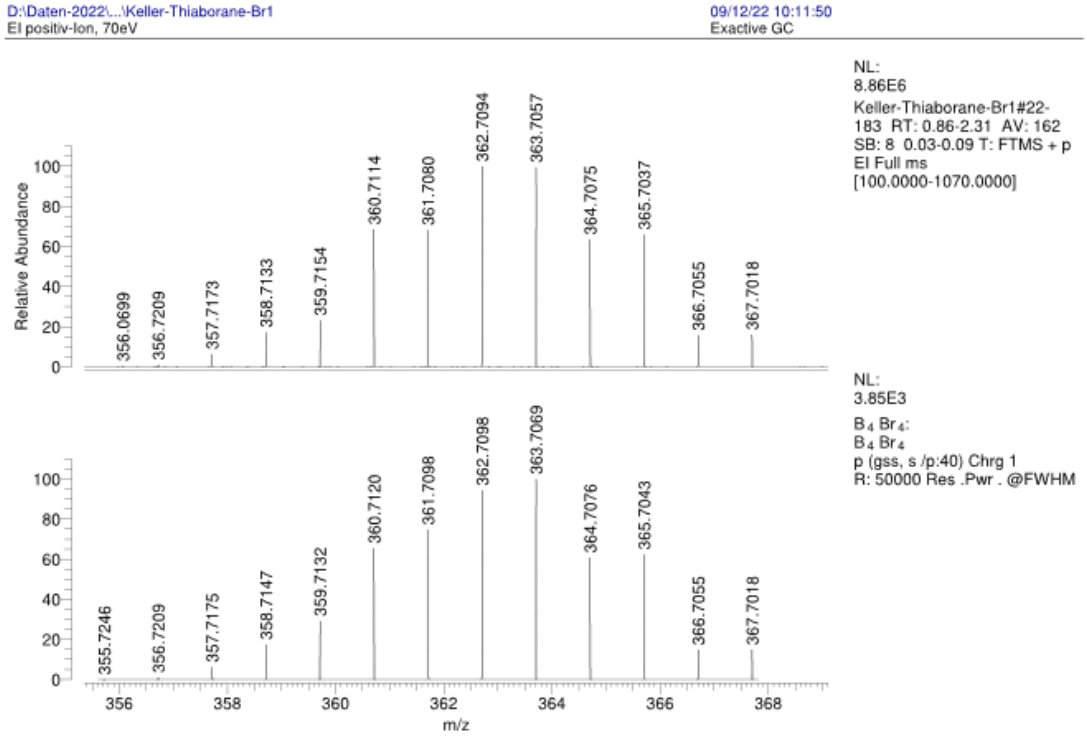

Figure S15. High resolution EI-MS of $[B_4Br_4]^+$ in the fragmentation of *closo*-SB_5Br_5 (**1**).

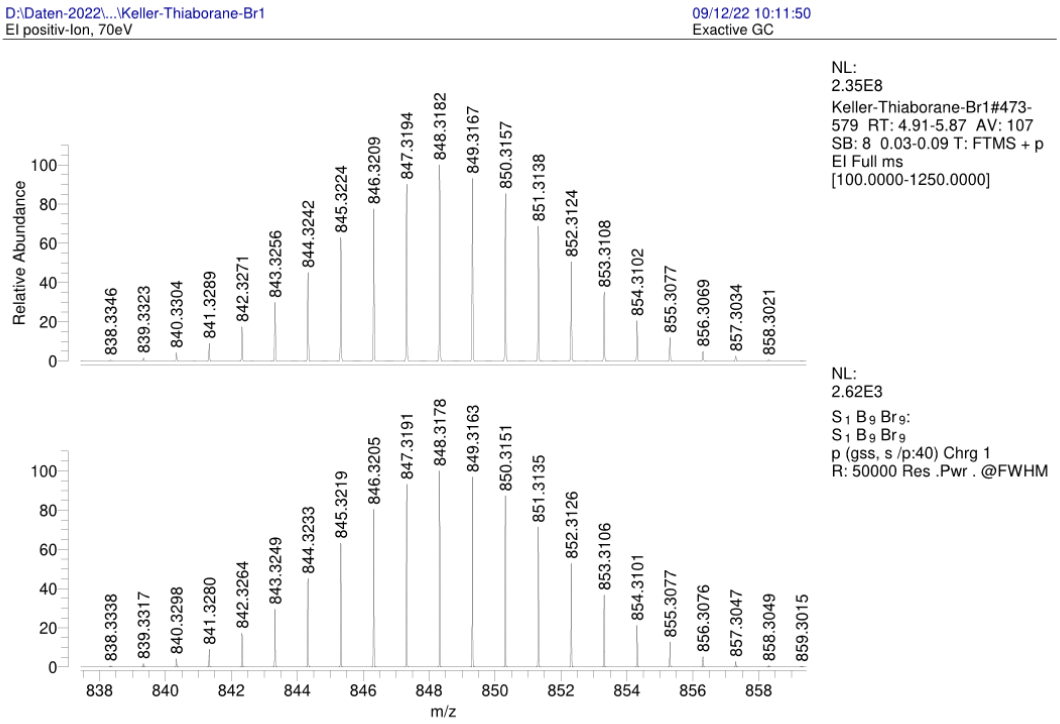

Figure S16. High resolution EI-MS of *closo*-1-SB_9Br_9 (**2**).

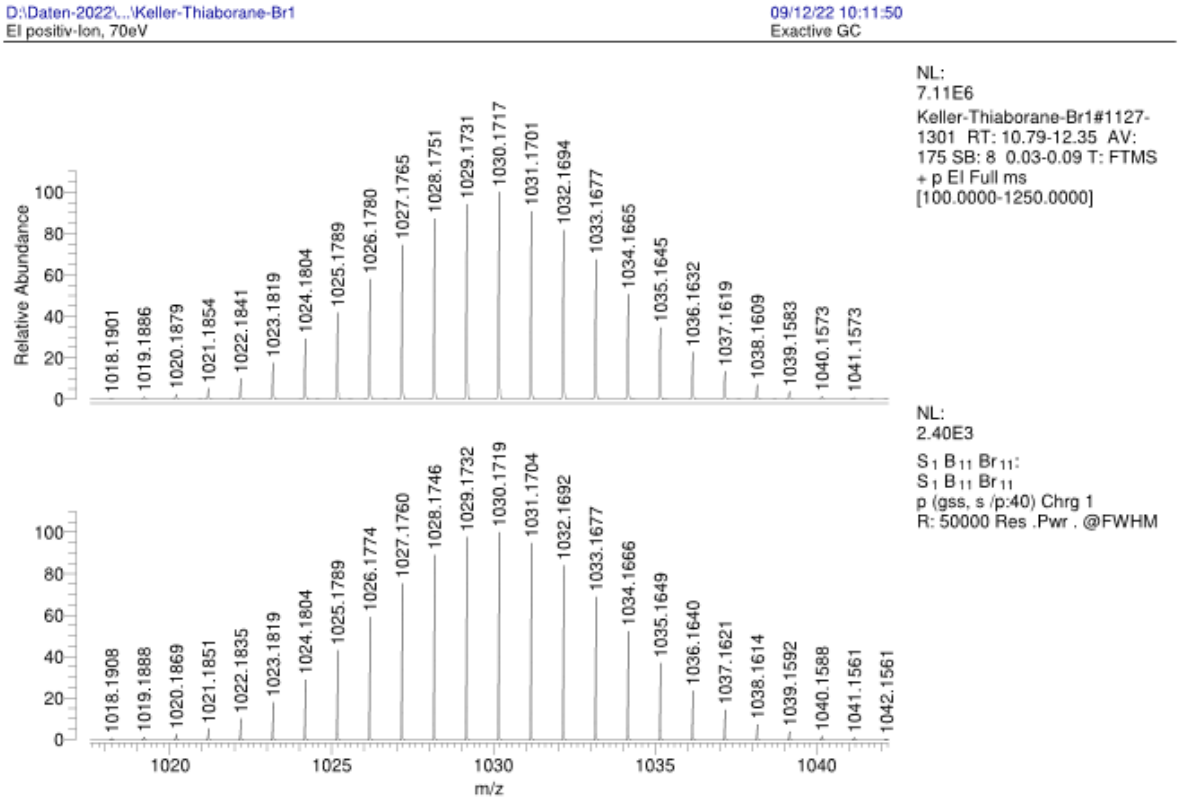

Figure S17. High resolution EI-MS of *closo*-$SB_{11}Br_{11}$ (**3**).

Figure S18. Sealed pyrolysis double-flask after reaction, before work-up.

References

1 D. F. Shriver, M. A. Drezdon in *The Manipulation of Air-Sensitive Compounds*, 2nd ed., John Wiley & Sons, New York, **1986**.

2 P. L. Timms, *Adv. Inorg. Chem. Radiochem.,* **1972**, *14*, 121.

3 W. Keller, J. Ballmann, M. B. Sárosi, J. Fanfrlík, D. Hnyk, *Angew. Chem. Int. Ed.* **2023**, *62*, e202219018.

4 F. Fehér, J. Kraemer, G. Rempe, *Z. Anorg. Allg. Chem.* **1955**, *279*, 18-27.

5 M. J. Frisch, G. W. Trucks, H. B. Schlegel, G. E. Scuseria, M. A. Robb, J. R. Cheeseman, G. Scalmani, V. Barone, B. Mennucci, G. A. Petersson, H. Nakatsuji, M. Caricato, X. Li, H. P. Hratchian, A. F. Izmaylov, J. Bloino, G. Zheng, J. L. Sonnenberg, M. Hada, M. Ehara, K. Toyota, R. Fukuda, J. Hasegawa, M. Ishida, T. Nakajima, Y. Honda, O. Kitao, H. Nakai, T. Vreven, J. A. Montgomery, Jr., J. E. Peralta, F. Ogliaro, M. Bearpark, J. J. Heyd, E. Brothers, K. N. Kudin, V. N. Staroverov, R. Kobayashi, J. Normand, K. Raghavachari, A. Rendell, J. C. Burant, S. S. Iyengar, J. Tomasi, M. Cossi, N. Rega, J. M. Millam, M. Klene, J. E. Knox, J. B. Cross, V. Bakken, C. Adamo, J. Jaramillo, R. Gomperts, R. E. Stratmann, O. Yazyev, A. J. Austin, R. Cammi, C. Pomelli, J. W. Ochterski, R. L. Martin, K. Morokuma, V. G. Zakrzewski, G. A. Voth, P. Salvador, J. J. Dannenberg, S. Dapprich, A. D. Daniels, Ö. Farkas, J. B. Foresman, J. V. Ortiz, J. Cioslowski, D. J. Fox, Gaussian 09, revision D.01, Gaussian, Inc., Wallingford CT, 2009.

6 a) G. te Velde, F. M. Bickelhaupt, E. J. Baerends, C. Fonseca Guerra, S. J. A. van Gisbergen, J. G. Snijders, T. Ziegler, *J. Comput. Chem.*, **2001**, *22*, 93; b) E. J. Baerends, J. Autschbach, A. Bérces, C. Bo, P. M. Boerrigter, L. Cavallo, D. P. Chong, L. Deng, R. M. Dickson, D. E. Ellis, L. Fan, T. H. Fischer, C. Fonseca Guerra, S. J. A. van Gisbergen, J. A. Groeneveld, O. V. Gritsenko, M. Grüning, F. E. Harris, P. van den Hoek, H. Jacobsen, G. van Kessel, F. Kootstra, E. van Lenthe, D. A. McCormack, V. P. Osinga, S. Patchkovskii, P. H. T. Philipsen, D. Post, C. C. Pye, W. Ravenek, P. Ros, P. R. T. Schipper, G. Schreckenbach, J. G. Snijders, M. Sola, M. Swart, D. Swerhone, G. te Velde, P. Vernooijs, L. Versluis, O. Visser, E. van Wezenbeek, G. Wiesenekker, S. K. Wolff, T. K. Woo, T. Ziegler, ADF2004.01, SCM, Theoretical Chemistry, Vrije Universiteit, Amsterdam, Netherlands, 2004.

7 (*a*) E. van Lenthe, E.J. Baerends and J.G. Snijders, *J. Chem. Phys.*, 1994, **101**, 9783; *(b)* E. van Lenthe, R. van Leeuwen, E.J. Baerends and J. G. Snijders, *Int. J. Quantum Chem.*, 1996, **57,** 281; (*c*) E. van Lenthe, E. J. Baerends, J. G. Snijders, *J. Chem. Phys.*, 1993, **99**, 4597.

8 E. van Lenthe, J. G. Snijders and E. J. Baerends, *J. Chem. Phys.*, 1996, **105**, 6505.

9 T. P. Onak, H. L. Landesman, R. E. Williams and I. Shapiro, *J. Phys. Chem.*, 1959, **63**, 1533.

10 MOLEKEL 4.3, P. Flükiger, H. P. Lüthi, S. Portmann, J. Weber, Swiss Center for scientific Computing, Manno, Switzerland, 2000, https://ugovaretto.github.io/molekel/ Accessed date 26.5.2020.

11 K. E. Riley, P. Tran, P. Lane, J. S. Murray and P. Politzer, *J. Comput. Sci*. 2016, **17**, 273.

12 G. Knizia, *J. Chem. Theory Comput.,* 2013, **9**, 4834.

13 *TURBOMOLE*, Version 7.3, 2018, a development of University of Karlsruhe and Forschungszentrum Karlsruhe GmbH, 1989-2017, TURBOMOLE GmbH, 2007.

14 K. Kabsch, in *International Tables for Crystallography*, Eds. Rossmann, M. G.; Arnold, E., *Vol. F*, Ch. 11.3, Kluwer Academic Publishers, Dordrecht, The Netherlands, 2001.

15 (*a*) *CrysAlisPro*, Agilent Technologies UK Ltd., Oxford, UK 2011-2014; (*b*) Rigaku Oxford Diffraction, Rigaku Polska Sp.z o.o., Wrocław, Poland 2015-2020.

16 *SCALE3 ABSPACK, CrysAlisPro*, Agilent Technologies UK Ltd., Oxford, UK 2011-2014.

17 R. H. Blessing, *Acta Cryst.* 1995, **A51**, 33.

18 W. R. Busing and H. A. Levy, *Acta Cryst.* 1957, **10**, 180.

19 O. V. Dolomanov, L. J. Bourhis, R. J. Gildea, J. A. K. Howard and H. Puschmann, H., *J. Appl. Cryst.* 2009,**42**, 339.

20 (*a*) G. M. Sheldrick, SHELXT, University of Göttingen and Bruker AXS GmbH, Karlsruhe, Germany, **2012**-**2018**; (*b*) M. Ruf and B.C. Noll, Application Note SC-XRD 503, Bruker AXS GmbH, Karlsruhe, Germany 2014; (*c*) G. M. Sheldrick, *Acta Cryst.* 2015, **A71**, 3.

21 *(a)* G. M. Sheldrick, *SHELXL-20xx*, University of Göttingen and Bruker AXS GmbH, Karlsruhe, Germany, 2012-2018; (*b*) G. M. Sheldrick, *Acta Cryst.* 2008, **A64**, 112; (*c*) G. M. Sheldrick, *Acta Cryst.* 2015, **C71**, 3.

22 A.L. Spek, *J. Appl. Cryst.* 2003, **36**, 7.